

Performance Comparison of Bounding Volume Hierarchies for GPU Ray Tracing

Daniel Meister

Advanced Micro Devices, Inc.

Jiří Bittner

Czech Technical University in Prague

Abstract

Ray tracing is an inherent component of modern rendering algorithms. The bounding volume hierarchy (BVH) is a commonly used acceleration data structure employed in most ray tracing frameworks. Through the last decade, many methods addressing ray tracing with bounding volume hierarchies have been proposed. However, most of these methods were typically compared to only one or two reference methods. The acceleration provided by a particular BVH depends heavily on its construction algorithm. Even experts in the field dispute which method is the best. To add more insight into this challenge, we empirically compare the most popular methods addressing BVHs in the context of GPU ray tracing. Moreover, we combine the construction algorithms with other enhancements such as spatial splits, ray reordering, and wide-BVHs. To estimate how close we are from the best performing BVH, we propose a novel method using global optimization with simulated annealing and combine it with the existing best performing BVH builders. For the sake of fairness and consistency, all methods are evaluated in a single unified framework, and we make all source code publicly available. We also study the correlation between tracing times and the estimated traversal cost induced by the surface area heuristic (SAH).

1. Introduction

Ray tracing stays at a core of many physically-based rendering algorithms. These algorithms model light transport by means of geometric optics, assuming that light travels instantaneously through the medium in straight lines. Ray tracing serves as an underlying engine to find the nearest intersections with scene geometry, to test visibility between two points, or to find all ray-scene intersections. The challenge is that we have to trace a large number of rays to achieve plausible results. Therefore, the scene geometry is arranged into various spatial data structures to accelerate the search for intersections. Modern ray tracing engines almost exclusively employ a bounding volume hierarchy (BVH) as an acceleration data structure as it provides

an excellent ray tracing performance, scalable construction times, and predictable memory footprint.

Over the last two decades, many different algorithms and methods addressing BVHs have been proposed. Nonetheless, they were tested only in a very limited setting, often against only one or very few reference algorithms. Moreover, using a combination of multiple techniques at once is usually simplified to a claim that individual techniques are orthogonal to each other, which might not be necessarily the truth in practice.

In this paper, we present a performance comparison of the BVH algorithms and techniques with a focus on GPU based methods. To gain more insight into how close the state-of-the-art techniques are from the optimal BVH for the given scene, we extend and combine the state-of-the-art BVH build methods that provided the best currently known BVHs. In particular, we propose a modification of the PRBVH method that includes a simulating annealing based global optimization and combine this method with the well-known SBVH method using spatial splits.

We mainly target offline rendering or static content in interactive or real-time applications, where the BVH is reused many times, and thus the build time becomes negligible with respect to trace times. Thus, our comparison focuses on the ray tracing performance that can be achieved using the particular BVH construction algorithm. To make the evaluation more informative, we also briefly discuss the BVH build times.

We compare the performance of ten different construction algorithms that are either existing well-known algorithms or their newly designed modifications and combinations. For each construction algorithm, we evaluate the ray tracing performance of resulting BVHs with different branching factors. We also study the influence of ray reordering on the BVH ray tracing performance. All evaluated methods are implemented in a single unified framework in order to make the comparison as fair as possible using a path tracer as a target rendering algorithm.

There are several works directly related to our paper. Meister et al. [2021] provided a comprehensive overview of bounding volume hierarchies methods. However, an empirical analysis is missing. Aila et al. [2013] provided a performance comparison focusing on the BVH quality metrics and their correlation with the actual tracing times limited to binary BVHs. Vinkler et al. [2016] conducted a performance comparison of bounding volume hierarchies and KD-trees on the GPU.

2. Background

In this section, we briefly describe the methods that we use for our comparison. For details, we refer to the individual papers or a recent survey by Meister et al. [2021].

2.1. Cost Model

We can estimate the quality of a particular BVH in terms of expected number of operations needed to find the nearest ray-triangle intersection. Using the surface area heuristic (SAH) [Goldsmith and Salmon 1987], we can express the cost function as follows:

$$c(N) = \begin{cases} c_T + \sum_{N_c} \frac{SA(N_c)}{SA(N)} c(N_c) & \text{if } N \text{ is interior node,} \\ c_I |N| & \text{otherwise.} \end{cases} \quad (1)$$

where $c(N)$ is the cost of a subtree with root N , N_c is a child of node N , $SA(N)$ is a surface area of the bounding box of node N , and $|N|$ is the number of triangles in node N . Constants c_T and c_I express the average cost of traversal and intersection steps, respectively. We can remove the recurrence by unrolling:

$$c(N) = \frac{1}{SA(N)} \left[c_T \sum_{N_i} SA(N_i) + c_I \sum_{N_l} SA(N_l) |N_l| \right], \quad (2)$$

where N_i and N_l are interior and leaf nodes, respectively. This model only roughly estimates what is happening in reality as it does not take into account many other factors such as the actual ray distribution, occlusions, underlying hardware architecture, or a particular rendering algorithm. However, most of the construction algorithms minimize this cost function (at least locally) to maximize the actual ray tracing performance. Notice that if we use one triangle per leaf, then the cost function reduces simply to the sum of surface areas of bounding boxes in interior nodes, which is the fact that some of the construction algorithms exploit.

Modern hardware architectures are equipped with SIMD units that allow processing multiple intersections tests at once, for example, in wide-BVHs, where a single ray is tested against multiple bounding boxes. Triangles in leaves are processed in similar fashion, and thus it is desirable to have the number of triangles aligned with the SIMD width as the number of executed intersection tests is equal to the SIMD width. Motivated by this fact, Wald et al. [2008] proposed a modified version of the cost model:

$$c(N) = \frac{1}{SA(N)} \left[c_T \sum_{N_i} SA(N_i) + c_I \sum_{N_l} SA(N_l) k \left\lceil \frac{|N_l|}{k} \right\rceil \right], \quad (3)$$

where k is the branching factor or the SIMD width. The modified cost mode penalizes leaves if their sizes are not aligned to k . Notice that we multiply the term by k to make c_T independent of k .

2.2. Construction

We first briefly describe the BVH construction algorithms evaluated in our paper.

Linear BVH *Linear BVH* (LBVH) is a very fast algorithm that reduces the problem of the BVH construction to the sorting problem. The idea is to sort triangles along a space-filling curve such as the Morton curve [Morton 1966]. The Morton curve subdivides space into a uniform grid, where the order along the curve is given by the Morton codes such that each Morton code corresponds to one cell of the grid. There is a simple mapping between cell coordinates and Morton codes by interleaving successive bits of cell coordinates. To construct a BVH over triangles, we approximate each triangle by a single point (e.g., the centroid of its bounding box), project it to the corresponding cell to compute its Morton code, and sort the triangles using the Morton codes as sorting keys. The Morton curve encodes an implicit binary BVH constructed by spatial median splits, where the most significant bit corresponds to the top-most split and so on. Karras [Karras 2012] proposed an algorithm that constructs the topology of this BVH in a single kernel launch, while the bounding boxes are computed separately in an additional kernel launch in a bottom-up fashion using atomic counters to prevent race conditions.

HLBVH LBVH is very fast, but it does not take into account the *surface area heuristic* (SAH), and thus the resulting BVHs are of rather inferior quality. To address this issue, several researchers proposed to combine LBVH with SAH, which is known as *hierarchical LBVH* (HLBVH) [Pantaleoni and Luebke 2010; Garanzha et al. 2011]. Garanzha et al. [2011] proposed to construct bottom levels by LBVH and then top levels in a top-down manner by binning. To reduce the workload for binning, the algorithm constructs the bottom levels by LBVH using less significant bits of Morton codes. Root nodes of bottom-level trees are further fed to binning using more significant bits as bin indices. Top-levels are constructed level by level using double buffering, where each level requires a separate kernel launch.

Parallel locally-ordered clustering Parallel locally-ordered clustering (PLOC) [Meister and Bittner 2018a] is a parallel bottom-up construction algorithm based on agglomerative clustering. The algorithm starts from the individual triangles considering them as clusters. Then, in each iteration, it merges multiple cluster pairs in parallel, repeating this until only one cluster remains, which corresponds to the root node. The algorithm employs the Morton curve to find the nearest neighbors efficiently.

Treelet restructuring Treelet restructuring (TRBVH) is a parallel optimization method that improves the quality of an existing BVH [Karras and Aila 2013]. The algorithm starts from the leaves and proceeds up to the root until a given treelet size is reached. Then, the treelets are restructured in order to locally minimize the BVH cost induced by a particular treelet. After the treelet is restructured, the algorithm continues one level above and repeats the process. To avoid race conditions, the node is only processed by the second thread (in the case of binary BVHs) using atomic counters to be sure that both children were already processed. Karras and Aila [2013]

restructured the treelet in an optimal way regarding the cost function using a dynamic programming approach. Later, Domingues and Pedrini [2015] showed that better results could be achieved using agglomerative clustering (ATRBVH), which is simple, and thus allows for restructuring large treelets. This approach provides BVHs of very good quality in reasonable times.

Parallel reinsertion Parallel reinsertion (PRBVH) [Meister and Bittner 2018b] is an optimization algorithm that iteratively modifies the BVH topology by local updates in order to decrease the global cost. The algorithm iteratively removes whole subtrees and inserts them into new positions while tracking the cost reduction for each such update. Thus, the cost function is systematically optimized as we know how exactly each update will influence the global cost, which is not the case of other methods that optimize the cost function only locally. The key observation is that we do not need to remove the node to find a new position. This fact allows us to search for new positions for all nodes in parallel, starting from original positions using simple state logic with parent links. To prevent topological conflicts, we employ atomic locks, prioritizing nodes with higher cost reduction. The algorithm always admits updates that reduce the global cost, which guarantees the global cost reduction. However, the algorithm may get stuck in a local minimum. Therefore, we propose to combine the algorithm with the simulated annealing that may also admit updates that temporally increase the global cost based on the stochastic decision to prevent getting stuck in local minima.

We use the simulated annealing in a similar manner as Kensler [2008] proposed for the rotation-based optimization. The acceptance probability is given by the Boltzmann factor:

$$P(\Delta d, T) = \begin{cases} \min(e^{-\Delta d/T}, 1) & T > 0 \\ 0 & T = 0, \end{cases} \quad (4)$$

where Δd is the difference of surface area of the proposed change, and T is the current temperature. The temperature is a clamped sine function:

$$T(i) = \max \left(0, -\sin \left(\frac{2\pi i}{f} \right) \right) T_{max} \frac{I-i}{I}, \quad (5)$$

where f is the frequency of the sine function, T_{max} is the hottest temperature allowed, i is the current iteration, and I is the total number of iterations.

Nonetheless, in the case of reinsertion, there are two factors that make it more complicated. The first factor is that the search space is huge, unlike the tree rotations, where the space is limited to the constant number of rotations. Similarly, that is why the method uses search space pruning [Meister and Bittner 2018b], which should also be stochastic, as the acceptance. However, we would search practically the whole space for high temperatures, which is not desirable. This effect is amplified through multiple iterations as the original position used for pruning is getting worse in each iteration during the heating phase. Thus, we use probability P (Equation 4) clamped

to $P_{pruning}$ (a parameter of typically small value). Note that for the pruning, we keep the best value found so far not necessarily corresponding to the last accepted value, which may also be negative.

The second factor is the parallel processing that causes two more issues. First, in the original algorithm [Meister and Bittner 2018b], there are two locking schemes to prevent race conditions: aggressive strategy (lock only nodes that are modified) and conservative strategy (lock the modified node and all nodes between them). The aggressive strategy is more efficient as it allows to perform more reinsertions in parallel as fewer nodes are locked. Nevertheless, this approach is not applicable for simulated annealing since inserting two subtrees into each other may result in a cycle, disconnecting the tree into two separate parts. In the case of hill climbing, these cases will not happen since they are automatically rejected as they do not provide any cost reduction. We resolve this issue by using the conservative strategy while the temperature is positive. Second, we need to resolve the conflicts between nodes. Prioritizing nodes with higher cost reductions would cause the deterministic reinsertions (with positive cost reduction) to discard most of the stochastic reinsertions (with negative cost reduction), resulting in practically no change, assuming that the BVH is already optimized. During the heating phase, we basically want to worsen the BVH to be able to improve it later when the temperature reaches zero again. Therefore, during the heating phase, we prioritize nodes with negative cost reduction.

Spatial splits BVH may adapt poorly to overlapping triangles with non-uniform sizes or long thin diagonal triangles. We can relax the restriction that each triangle is referenced only once, allowing us to achieve tighter bounding boxes at the cost of a higher number of triangle references in leaves. SBVH [Stich et al. 2009] is a top-down construction algorithm that allows, besides standard objects, also spatial splits in the same manner as in the KD-tree construction, selecting one that minimizes the BVH cost. This algorithm provides BVHs of the highest quality a cost of slower construction and more difficult parallelization. Unlike standard BVHs, BVHs with spatial splits cannot be easily updated by refitting the bounding volumes, which might cause issues in handling dynamic scenes.

2.3. Traversal

Traversal on the GPU might be challenging due to warp divergence and incoherent memory accesses. Aila and Laine [2009] proposed a stack-based traversal algorithm with persistent warps and dynamic fetch. The algorithm spawns an optimal number of warps that fetch rays from the global queue. To prevent warp divergence, the traversal is divided into two independent loops processing interior and leaf nodes separately (i.e., the *while-while* traversal). If all active threads in the warp reached leaf nodes, then the algorithm switches to the second while loop and tests the triangles in the leaf nodes. Dynamic fetch allows to fetch new rays if a certain number of threads are

inactive to keep parallel resources occupied enough.

Lier et al. [2018] proposed a stack-based traversal algorithm for wide-BVHs. The idea is to process a single node by multiple threads in a similar manner as nodes are processed on the CPU using SIMD processing.

2.4. Ray Reordering

Ray reordering is a technique that regroups the rays in order to increase control flow, cache-hit ratios, and decrease warp divergence [Meister et al. 2020]. Using ray reordering only pays off if the performance gain outweighs additional overhead. Ray reordering is typically implemented by sorting the rays along the Morton curve. The crucial part is how the ray as a 5D entity is encoded into a Morton code, which is not as straightforward as for 3D points.

3. Implementation

In this section, we provide implementations details of the evaluated methods. Most of the tested methods have publicly available implementations. However, to provide a fair comparison, we have to use the same setting for all methods, which might be difficult in different frameworks. Thus, we created a single unified framework with publicly available implementations of the algorithm integrated into it. Our framework is based on Aila’s ray tracing framework [Aila and Laine 2009].

Aila’s framework contains high-performance traversal kernels for binary BVHs. To support wide-BVHs, we adopted the publicly available implementations of the method proposed by Lier et al. [2018]. In the original version of these kernels, the leaf size is limited to the branching factor of the BVHs. We modified the kernels to support arbitrary leaf sizes.

For LBVH [Karras 2012] and HLBVH [Garanzha et al. 2011], we use our implementation. For PLOC [Meister and Bittner 2018a], ATRBVH [Domingues and Pedrini 2015], and PRBVH [Meister and Bittner 2018b], we integrated publicly available implementations into our framework. For SBVH [Stich et al. 2009], we use the implementation that is available in Aila’s framework [Aila and Laine 2009]. We implemented the collapsing algorithm of Ylitie et al. [2017] to convert binary BVHs to wide ones with adaptive leaf sizes while minimizing the BVH cost (Equation 3). The data layout (i.e., how nodes are stored in the memory) has a significant impact on the actual ray tracing performance. Various methods provide BVHs in different data layouts. Hence, to provide a fair comparison, we transform each BVH to the bread-first-search (BFS) layout prior to the actual ray tracing. The nodes are stored in the *array-of-structures* fashion, where each node contains bounding boxes of children and child indices, taking $32k$ bytes per node for k -ary BVHs.

We implemented a wavefront path tracing with the next event estimation on top

of our ray tracing framework. We can optionally use ray reordering to sort secondary and shadow rays. In the case of sorting, we access the rays indirectly through sorted indices in the traversal kernels to minimize the overhead caused by the actual reordering of the rays [Meister et al. 2020]. We use compacted Aila’s method to compute the Morton codes. We employ the radix sort algorithm by Merril and Grimshaw [2011] for both construction algorithms and ray reordering.

4. Results and Discussion

We evaluated selected methods on 12 scenes of various complexity (see Figure 2). The path tracer uses 32 samples per pixel with the next event estimation using two shadow rays per hit with the maximum recursion depth 8. We do not employ Russian roulette and so in closed interior scenes the maximum recursion depth is often reached; in exterior scenes, the light paths are significantly shorter. All images were rendered in the 1024×768 resolution. The reported numbers are averaged over three different camera views to reduce the influence of view dependency. We evaluated all methods with and without ray reordering. The reordering overhead is included in trace times for the sake of fairness; both the traversal and the reordering are implemented on the same platform, and thus we expect that similar performance results could be obtained using hardware accelerated units for reordering and tracing. All experiments were executed on the AMD Ryzen 9 5950X CPU and AMD Radeon 6800 XT GPU and implemented using HIP as part of ROCm 4.4.

We used six construction methods for our experiments: LBVH, HLBVH, PLOC, ATRBVH, PRBVH, and SBVH. We used 60-bit Morton code for LBVH, HLBVH, and PLOC. For HLBVH, we used 15 bits for the SAH splits. For PLOC, we used the search radius of 100. For ATRBVH, we used 20 iterations and LBVH for the initial construction. For PRBVH, we used four configurations: PRBVH (LBVH as a base BVH with hill climbing), PRBVH^A (LBVH as a base BVH with simulated annealing), PRBVH_S (SBVH as a base BVH with hill-climbing), and PRBVH_S^A (SBVH as a base BVH with simulated annealing). We used $f = 50$, $T_{max} = 1$, $I = 3000$ and $P_{pruning} = 0.01$ for the simulated annealing. For SBVH, we used 128 bins for spatial splitting. We can disable spatial splits, which is equivalent to the standard full sweep top-down construction (denoted by SAH). We used $c_T = 3$ and $c_I = 2$ for the BVH cost computation and optimization. These values were established by experimental evaluation as maximizing the trace performance on the target platform. We evaluated all methods using three different branching factors: 2 (binary BVHs), 4 (quaternary BVHs), and 8 (octal BVHs) (these branching factors are supported by the existing traversal kernels).

We present a compact summary of the results in Tables 1 and 3, where the values are averaged over all scenes. A detailed overview of results is in Tables 4, 5, and

[6](#) for branching factors 2, 4, and 8, respectively. For each method, we report the BVH cost and trace performance for secondary and shadow rays with and without ray reordering.

4.1. BVH Cost

PRBVH_S^A achieves the lowest BVH cost across all configurations, showing that SBVH can be optimized even further (about 7% on average for binary BVHs). We can observe that the improvement of the BVH cost achieved by simulated annealing is only marginal. Therefore, we assume that the resulting BVHs are close to the optimal SAH cost for the given scene. Interestingly, PRBVH and PRBVH^A provide binary BVHs of similar costs as SBVH. SAH, which was for a long time considered as a reference solution, provides BVHs with relatively high costs on average, higher than PLOC and ATRBVH.

4.2. Trace Speed

The results show that PRBVH_S , PRBVH_S^A , and SBVH achieve the highest trace performance. In most cases, PRBVH_S performs better than SBVH with one exception of secondary rays with binary BVHs, where it achieves slightly higher trace speed than PRBVH_S and PRBVH_S^A . The results indicate that PRBVH can improve an input SBVH in some cases. Interestingly, PRBVH_S^A is slightly worse than PRBVH_S . An explanation could be that the simulated annealing breaks optimized top-level splits of SBVH (see Section 4.3).

We can observe that the trace performance drops significantly with increasing branching factor for both secondary and shadow rays. This behavior is the most pronounced for primary rays that exhibit highest coherence (the tables do not show numbers for primary rays, as these constitute a small fraction of the rendering times). One reason might be that wide-BVHs use different traversal algorithm [[Lier et al. 2018](#)] than for binary BVHs [[Aila and Laine 2009](#)]. For quaternary and octal BVHs, PRBVH_S and PRBVH_S^A outperform SBVH for both secondary and shadow rays. GPU ray tracing is memory bandwidth limited, and thus to achieve higher trace performance for higher branching factors, it is necessary to employ some kind of node compression [[Ylitie et al. 2017](#)], which was not used in our comparison.

Table 1 shows that using spatial splitting pays off overall, improving trace performance about by 24% for secondary rays and 12% for shadow rays on average. However, the speedup provided by spatial splits depends heavily on a particular scene. There is a rather marginal improvement for finely tessellated scenes such as Conference, Happy Buddha, and Hairball. On the other hand, for a complex scene such as Powerplant, the speedup is almost threefold.

4.3. Cost and Trace Speed Correlation

There is a well-known fact that there is a discrepancy between the BVH cost and the actual trace performance [Aila et al. 2013]. In other words, cost reduction does not necessarily mean trace performance improvement. Top-down builders, such as SAH and SBVH, provide BVHs with higher costs than other approaches, but the top levels are locally well optimized, which is important as most of the time during the traversal is spent in the top levels as they are visited by almost all rays. To quantize this fact, we compute the ratio between trace time and cost, which expresses the time needed for a unit cost (see Table 2). These values are averaged over all scenes. The values are normalized prior to averaging by a value given by LBVH of the corresponding branching factor. Top-down builders such as SAH and SBVH have lower values, while optimization algorithms such as PRBVH and bottom-up algorithms as PLOC have higher values. These values can be considered as a correction to the actual cost values. By multiplying the cost by these values, we can obtain a corrected cost that actually corresponds to the trace times. We also plot normalized trace times and normalized BVH costs in Figure 1 to see correlation between these two quantities.

4.4. Influence of Ray Reordering

Table 1 indicates that using ray reordering pays off on average, providing a speedup 7% for secondary and 8% for shadow rays. Particularly, ray reordering improves trace performance for Crytek Sponza (23% secondary rays and 39% shadow rays), Conference (15% secondary rays and 37% shadow rays), and San Miguel (14% secondary rays and 26% shadow rays) using binary BVHs. Ray reordering typically benefits from using larger ray batches as it is more likely to extract coherence from a large number of rays. Furthermore, the speed of the ray sorting algorithm, i.e., number of rays sorted per second, increases with more rays. Thus, it pays off to use ray reordering for complex scenes (e.g., Hairball) or architectural scenes (e.g., San Miguel). On the other hand, in object-like scenes (e.g., Happy Buddha), most of the rays escape the scene after the first bounce, and further bounces are generated only in concave regions, generating only a few secondary rays. Thus, it is difficult to extract some coherence from a small number of rays and fully utilize parallel resources.

However, we can observe that the effect of ray reordering decreases with an increasing branching factor, especially for shadow rays. For example, ray reordering improves trace performance for shadow rays in San Miguel by 26% for binary BVHs, 18% for quaternary BVHs, and 11% for octal BVHs using PRBVH_S. One reason might be again that for wide-BVHs, we use a completely different trace kernel [Lier et al. 2018] than for binary BVHs [Aila and Laine 2009]. Another reason might be that in wide-BVHs, we visit fewer nodes during the traversal, which results in fewer memory accesses, decreasing the importance of ray coherence.

| Br. factor | Rays | LBVH | HLBVH | PLOC | ATRBVH | PRBVH | PRBVH ^A | PRBVH _S | PRBVH _S ^A | SAH | SBVH |
|--------------------|-----------|------|-------|------|--------|-------|--------------------|--------------------|---------------------------------|------|-------------|
| without reordering | | | | | | | | | | | |
| 2 | Secondary | 1.00 | 1.10 | 1.25 | 1.39 | 1.45 | 1.48 | 1.85 | 1.84 | 1.43 | 1.86 |
| | Shadow | 1.00 | 1.08 | 1.32 | 1.39 | 1.47 | 1.47 | 1.66 | 1.64 | 1.40 | 1.63 |
| 4 | Secondary | 1.04 | 1.16 | 1.31 | 1.39 | 1.49 | 1.50 | 1.76 | 1.74 | 1.41 | 1.73 |
| | Shadow | 0.92 | 1.02 | 1.19 | 1.24 | 1.32 | 1.32 | 1.40 | 1.39 | 1.23 | 1.36 |
| 8 | Secondary | 0.98 | 1.08 | 1.21 | 1.31 | 1.40 | 1.42 | 1.58 | 1.57 | 1.30 | 1.54 |
| | Shadow | 0.86 | 0.94 | 1.07 | 1.12 | 1.17 | 1.18 | 1.23 | 1.22 | 1.10 | 1.19 |
| with reordering | | | | | | | | | | | |
| 2 | Secondary | 1.09 | 1.20 | 1.36 | 1.50 | 1.56 | 1.58 | 1.98 | 1.96 | 1.54 | 2.01 |
| | Shadow | 1.23 | 1.33 | 1.58 | 1.64 | 1.75 | 1.72 | 1.89 | 1.87 | 1.66 | 1.87 |
| 4 | Secondary | 1.17 | 1.30 | 1.44 | 1.53 | 1.62 | 1.63 | 1.90 | 1.88 | 1.54 | 1.88 |
| | Shadow | 1.06 | 1.16 | 1.33 | 1.38 | 1.45 | 1.45 | 1.51 | 1.50 | 1.37 | 1.48 |
| 8 | Secondary | 1.08 | 1.19 | 1.31 | 1.41 | 1.50 | 1.52 | 1.68 | 1.65 | 1.41 | 1.64 |
| | Shadow | 0.92 | 0.99 | 1.12 | 1.16 | 1.22 | 1.22 | 1.26 | 1.25 | 1.15 | 1.22 |

Table 1. Relative ray tracing performance of BVHs build using the tested construction algorithms. The table shows relative trace speed for tracing secondary and shadow rays with and without ray sorting using BVHs of different branching factors. The trace speed is normalized by the speed of the binary LBVH and averaged over all tested scenes.

| Br. factor | Statistic | LBVH | HLBVH | PLOC | ATRBVH | PRBVH | PRBVH ^A | PRBVH _S | PRBVH _S ^A | SAH | SBVH |
|------------|---------------------|------|-------|------|--------|-------|--------------------|--------------------|---------------------------------|------|------|
| 2 | BVH cost | 1.00 | 0.83 | 0.70 | 0.65 | 0.61 | 0.60 | 0.55 | 0.55 | 0.68 | 0.59 |
| | Second. rays | 1.00 | 1.11 | 1.21 | 1.18 | 1.21 | 1.21 | 1.11 | 1.12 | 1.07 | 1.02 |
| | Shadow rays | 1.00 | 1.13 | 1.14 | 1.18 | 1.19 | 1.21 | 1.22 | 1.24 | 1.10 | 1.14 |
| | Second. rays reord. | 0.92 | 1.03 | 1.12 | 1.10 | 1.14 | 1.16 | 1.05 | 1.07 | 1.01 | 0.96 |
| | Shadow rays reord. | 0.84 | 0.95 | 0.98 | 1.03 | 1.03 | 1.07 | 1.10 | 1.11 | 0.95 | 1.01 |
| 4 | BVH cost | 1.00 | 0.88 | 0.77 | 0.73 | 0.70 | 0.69 | 0.62 | 0.62 | 0.74 | 0.64 |
| | Second. rays | 1.00 | 1.03 | 1.08 | 1.06 | 1.04 | 1.04 | 1.07 | 1.08 | 1.03 | 1.06 |
| | Shadow rays | 1.00 | 1.03 | 1.04 | 1.05 | 1.04 | 1.05 | 1.16 | 1.17 | 1.05 | 1.16 |
| | Second. rays reord. | 0.89 | 0.93 | 0.98 | 0.97 | 0.96 | 0.97 | 1.00 | 1.01 | 0.94 | 0.98 |
| | Shadow rays reord. | 0.87 | 0.92 | 0.94 | 0.95 | 0.95 | 0.97 | 1.08 | 1.09 | 0.94 | 1.07 |
| 8 | BVH cost | 1.00 | 0.92 | 0.81 | 0.79 | 0.76 | 0.75 | 0.67 | 0.67 | 0.76 | 0.66 |
| | Second. rays | 1.00 | 0.99 | 1.04 | 0.99 | 0.96 | 0.96 | 1.02 | 1.03 | 1.01 | 1.06 |
| | Shadow rays | 1.00 | 1.00 | 1.02 | 1.01 | 1.00 | 1.00 | 1.12 | 1.13 | 1.06 | 1.18 |
| | Second. rays reord. | 0.91 | 0.90 | 0.96 | 0.92 | 0.90 | 0.90 | 0.96 | 0.97 | 0.94 | 0.99 |
| | Shadow rays reord. | 0.94 | 0.95 | 0.98 | 0.97 | 0.97 | 0.97 | 1.10 | 1.11 | 1.02 | 1.14 |

Table 2. Comparison of the BVH costs and the average trace times per a unit BVH cost (i.e., trace time divided by the BVH cost). The values are normalized prior averaging by a value given by LBVH of the corresponding BVH branching factor.

5. Conclusion and Future Work

We provided an overview of the state-of-the-art BVH construction methods together with their extensive empirical performance comparison. In particular, we compared the various state of the art construction algorithms, spatial splitting, ray reordering, and wide-BVHs. We also measured the discrepancy between trace times and BVH costs. We found out that the best results are provided by binary BVHs constructed by SBVH, while ray reordering pays off in most of the cases. We also showed that parallel reinsertion in combination with simulated annealing can provide slightly better costs than parallel reinsertion itself.

| Scene | LBVH | HLBVH | PLOC | ATRBVH | PRBVH | PRBVH^A | PRBVH_S | PRBVH_S^A | SAH | SBVH |
|-----------------|------|-------|------|--------|-------|------------------|------------------|--------------------|-------|--------|
| Sibenik | 2.0 | 7.5 | 17.2 | 8.2 | 22.0 | 3843 | 2811 | 7269 | 281 | 2801 |
| Crytek Sponza | 2.3 | 7.9 | 20.9 | 12.8 | 52.0 | 11218 | 6494 | 19427 | 1266 | 6467 |
| Conference | 2.6 | 7.9 | 21.2 | 15.2 | 107 | 25215 | 4347 | 30759 | 1561 | 4271 |
| Gallery | 3.9 | 11.0 | 22.0 | 21.3 | 99.0 | 37018 | 20904 | 63757 | 4915 | 20851 |
| Happy Buddha | 4.2 | 11.3 | 26.6 | 22.9 | 123 | 40294 | 19062 | 62096 | 5494 | 19004 |
| Sodahall | 7.3 | 15.9 | 35.2 | 50.1 | 453 | 101822 | 29896 | 140533 | 12024 | 29575 |
| Hairball | 8.7 | 17.4 | 55.1 | 60.7 | 543 | 154483 | 219852 | 682155 | 14049 | 218225 |
| Crown | 15.5 | 26.1 | 66.5 | 110 | 799 | 223908 | 51998 | 292668 | 30168 | 51623 |
| Pompeii | 17.5 | 31.7 | 63.5 | 145 | 3500 | 325587 | 74168 | 421387 | 31482 | 73344 |
| San Miguel | 24.4 | 38.5 | 96.3 | 183 | 2309 | 531512 | 78568 | 552505 | 51540 | 77480 |
| Vienna | 27.1 | 43.2 | 82.7 | 207 | 4254 | 536393 | 77383 | 612130 | 53257 | 76493 |
| Powerplant | 36.7 | 53.0 | 129 | 292 | 5752 | 837940 | 147898 | 907441 | 88119 | 146337 |
| Avg. build time | 1.0 | 2.3 | 5.6 | 6.6 | 76.1 | 13720 | 5237 | 22134 | 1444 | 5196 |

Table 3. The table shows build times in milliseconds for binary BVHs. The last line shows average build times; times are normalized prior averaging by a value given by LBVH.

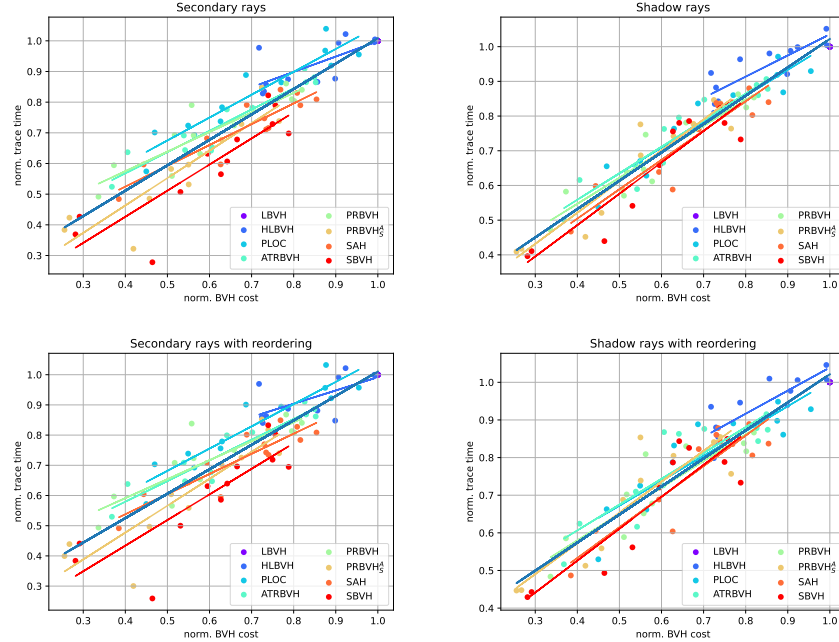


Figure 1. Correlation between BVH costs and tracing times for secondary and shadow rays using binary BVHs. Both BVH cost and trace times are normalized by LBVH.

The results indicate several promising directions for future work. One obvious direction would be a fast construction using spatial splits while keeping the quality of SBVH. Another interesting direction might be a hybrid construction using top-down construction for top levels and bottom-up construction for bottom levels. On a similar note, we could modify PRBVH to penalize or completely disable updates in top levels to preserve top splits provided by SBVH. Furthermore, during the conversion to wide-

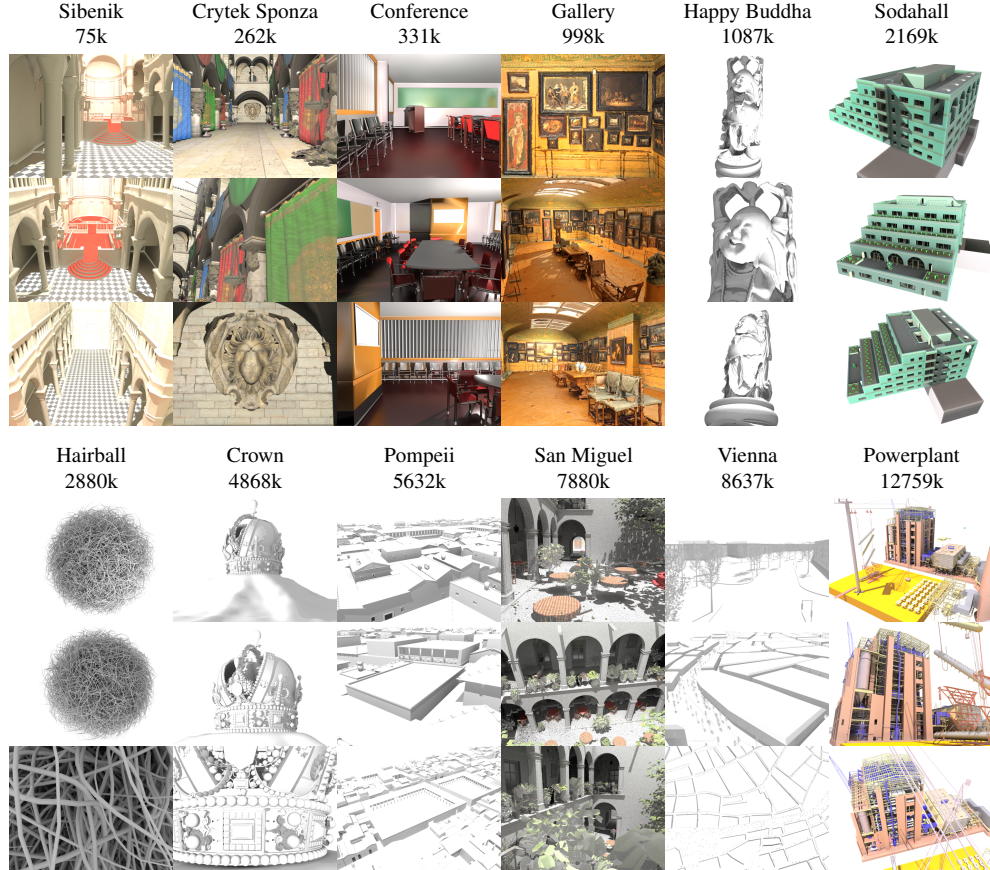


Figure 2. Rendered images of 12 tested scenes in resolution 1024×768 . We use three representative views for each scene.

BVH, some nodes are discarded. Thus, it makes sense to focus the optimization only on the nodes that remain and not on the discarded nodes. However, as was pointed by Meister et al. [2021], this is a difficult challenge as the cost function in wide-BVHs is piece-wise constant (i.e., some of the topological updates do not change the cost value), which makes the navigation in the search space more difficult.

Simulated annealing could also be used with other BVH construction methods such as treelet restructuring. Moreover, in simulated annealing, we clamp the probability used for pruning to a constant and prioritize nodes with negative values during the heating phase. In both cases, we could use more sophisticated approaches. We leave these problems as future work.

Acknowledgements

We would like to thank Jakub Černý for fruitful discussions and valuable comments. We thank Seth Teller for providing the Sodahall scene, Peter Wonka and Michael

| Scene | Statistic | LBVH | HLBVH | PLOC | ATRBVH | PRBVH | PRBVH ^A | PRBVH _S | PRBVH _S ^A | SAH | SBVH |
|-------------------------------------|---------------------|-------------|-------------|-------------|-------------|-------------------|--------------------|--------------------|---------------------------------|-------------|-------------------|
| Sibenik #triangles 75k | BVH cost | 177 (1.00) | 139 (0.79) | 136 (0.77) | 124 (0.70) | 116 (0.66) | 114 (0.65) | 112 (0.63) | 111 (0.63) | 129 (0.73) | 118 (0.67) |
| | Second. rays | 261 (1.00) | 299 (1.14) | 302 (1.16) | 334 (1.28) | 361 (1.38) | 364 (1.39) | 389 (1.49) | 386 (1.48) | 349 (1.34) | 385 (1.47) |
| | Shadow rays | 604 (1.00) | 627 (1.04) | 702 (1.16) | 712 (1.18) | 773 (1.28) | 803 (1.33) | 814 (1.35) | 814 (1.35) | 721 (1.19) | 769 (1.27) |
| | Second. rays reord. | 311 (1.19) | 351 (1.34) | 348 (1.33) | 385 (1.47) | 415 (1.59) | 418 (1.60) | 449 (1.72) | 443 (1.70) | 405 (1.55) | 447 (1.71) |
| | Shadow rays reord. | 891 (1.47) | 941 (1.56) | 1000 (1.66) | 1016 (1.68) | 1073 (1.78) | 1107 (1.83) | 1103 (1.83) | 1107 (1.83) | 1035 (1.71) | 1078 (1.79) |
| Crytek Sponza #triangles 262k | BVH cost | 268 (1.00) | 195 (0.73) | 168 (0.63) | 162 (0.60) | 155 (0.58) | 153 (0.57) | 149 (0.56) | 148 (0.55) | 198 (0.74) | 168 (0.63) |
| | Second. rays | 159 (1.00) | 190 (1.20) | 215 (1.36) | 247 (1.56) | 251 (1.58) | 278 (1.75) | 298 (1.88) | 298 (1.88) | 222 (1.40) | 281 (1.77) |
| | Shadow rays | 401 (1.00) | 455 (1.13) | 553 (1.38) | 603 (1.50) | 656 (1.63) | 656 (1.63) | 583 (1.45) | 584 (1.46) | 481 (1.20) | 531 (1.32) |
| | Second. rays reord. | 205 (1.29) | 238 (1.50) | 271 (1.71) | 302 (1.91) | 313 (1.97) | 336 (2.11) | 368 (2.32) | 366 (2.31) | 279 (1.76) | 349 (2.20) |
| | Shadow rays reord. | 597 (1.49) | 678 (1.69) | 758 (1.89) | 822 (2.05) | 880 (2.19) | 885 (2.21) | 808 (2.02) | 807 (2.01) | 708 (1.77) | 758 (1.89) |
| Conference #triangles 331k | BVH cost | 154 (1.00) | 112 (0.72) | 85 (0.55) | 83 (0.54) | 80 (0.52) | 79 (0.51) | 79 (0.51) | 92 (0.59) | 92 (0.60) | |
| | Second. rays | 278 (1.00) | 327 (1.18) | 384 (1.38) | 402 (1.45) | 401 (1.44) | 403 (1.45) | 487 (1.75) | 477 (1.72) | 407 (1.47) | 439 (1.58) |
| | Shadow rays | 525 (1.00) | 648 (1.24) | 783 (1.49) | 799 (1.52) | 821 (1.57) | 833 (1.59) | 898 (1.71) | 892 (1.70) | 821 (1.57) | 797 (1.52) |
| | Second. rays reord. | 331 (1.19) | 385 (1.39) | 449 (1.62) | 468 (1.68) | 468 (1.69) | 469 (1.69) | 562 (2.03) | 549 (1.98) | 468 (1.69) | 525 (1.89) |
| | Shadow rays reord. | 836 (1.59) | 1047 (1.99) | 1153 (2.20) | 1178 (2.25) | 1191 (2.27) | 1208 (2.30) | 1234 (2.35) | 1215 (2.32) | 1214 (2.31) | 1160 (2.21) |
| Gallery #triangles 998k | BVH cost | 197 (1.00) | 195 (0.99) | 188 (0.95) | 167 (0.85) | 161 (0.82) | 157 (0.80) | 146 (0.74) | 146 (0.74) | 159 (0.81) | 149 (0.76) |
| | Second. rays | 148 (1.00) | 149 (1.00) | 155 (1.05) | 168 (1.13) | 176 (1.19) | 178 (1.20) | 187 (1.26) | 186 (1.25) | 179 (1.20) | 188 (1.27) |
| | Shadow rays | 355 (1.00) | 338 (0.95) | 382 (1.08) | 392 (1.10) | 416 (1.17) | 416 (1.17) | 427 (1.20) | 424 (1.20) | 403 (1.14) | 426 (1.20) |
| | Second. rays reord. | 165 (1.11) | 165 (1.11) | 172 (1.16) | 186 (1.25) | 196 (1.32) | 197 (1.33) | 202 (1.37) | 202 (1.36) | 199 (1.34) | 205 (1.38) |
| | Shadow rays reord. | 479 (1.35) | 458 (1.29) | 516 (1.45) | 524 (1.48) | 553 (1.56) | 553 (1.56) | 563 (1.58) | 561 (1.58) | 539 (1.52) | 564 (1.59) |
| Happy Buddha #triangles 1087k | BVH cost | 204 (1.00) | 184 (0.91) | 178 (0.87) | 168 (0.83) | 159 (0.78) | 156 (0.76) | 148 (0.73) | 147 (0.72) | 156 (0.77) | 150 (0.74) |
| | Second. rays | 105 (1.00) | 105 (1.01) | 108 (1.03) | 115 (1.10) | 122 (1.16) | 122 (1.16) | 125 (1.20) | 124 (1.18) | 124 (1.19) | 127 (1.22) |
| | Shadow rays | 159 (1.00) | 161 (1.01) | 173 (1.09) | 179 (1.12) | 184 (1.16) | 186 (1.17) | 189 (1.19) | 188 (1.18) | 189 (1.19) | 193 (1.21) |
| | Second. rays reord. | 98 (0.93) | 98 (0.94) | 102 (0.97) | 107 (1.02) | 112 (1.07) | 112 (1.07) | 116 (1.11) | 115 (1.09) | 115 (1.10) | 117 (1.12) |
| | Shadow rays reord. | 135 (0.85) | 138 (0.87) | 150 (0.94) | 154 (0.97) | 157 (0.98) | 158 (0.99) | 162 (1.02) | 160 (1.01) | 161 (1.01) | 165 (1.04) |
| Sodahall #triangles 2169k | BVH cost | 254 (1.00) | 217 (0.86) | 174 (0.69) | 163 (0.64) | 143 (0.56) | 141 (0.56) | 140 (0.55) | 140 (0.55) | 186 (0.73) | 163 (0.64) |
| | Second. rays | 220 (1.00) | 255 (1.15) | 248 (1.13) | 284 (1.29) | 319 (1.45) | 319 (1.45) | 375 (1.70) | 370 (1.68) | 310 (1.41) | 363 (1.65) |
| | Shadow rays | 603 (1.00) | 615 (1.02) | 721 (1.20) | 758 (1.26) | 808 (1.34) | 808 (1.34) | 786 (1.30) | 777 (1.29) | 727 (1.21) | 773 (1.28) |
| | Second. rays reord. | 240 (1.09) | 272 (1.23) | 266 (1.21) | 300 (1.36) | 331 (1.50) | 332 (1.50) | 378 (1.72) | 373 (1.69) | 323 (1.46) | 375 (1.70) |
| | Shadow rays reord. | 667 (1.11) | 660 (1.09) | 750 (1.24) | 772 (1.28) | 824 (1.37) | 809 (1.34) | 792 (1.31) | 781 (1.29) | 759 (1.26) | 790 (1.31) |
| Hairball #triangles 2880k | BVH cost | 1233 (1.00) | 1225 (0.99) | 1082 (0.88) | 1051 (0.85) | 981 (0.80) | 979 (0.79) | 835 (0.68) | 834 (0.68) | 1054 (0.85) | 925 (0.75) |
| | Second. rays | 74 (1.00) | 74 (1.00) | 71 (0.96) | 86 (1.16) | 91 (1.24) | 89 (1.20) | 104 (1.41) | 101 (1.37) | 91 (1.24) | 101 (1.37) |
| | Shadow rays | 170 (1.00) | 169 (1.01) | 175 (1.03) | 193 (1.14) | 202 (1.19) | 201 (1.18) | 221 (1.30) | 218 (1.29) | 202 (1.19) | 217 (1.28) |
| | Second. rays reord. | 79 (1.07) | 80 (1.08) | 77 (1.04) | 92 (1.25) | 98 (1.32) | 96 (1.30) | 112 (1.52) | 109 (1.48) | 98 (1.33) | 110 (1.49) |
| | Shadow rays reord. | 192 (1.13) | 191 (1.12) | 202 (1.19) | 219 (1.29) | 229 (1.35) | 228 (1.34) | 247 (1.46) | 243 (1.43) | 229 (1.35) | 243 (1.43) |
| Crown #triangles 4868k | BVH cost | 76 (1.00) | 70 (0.92) | 68 (0.89) | 63 (0.83) | 61 (0.80) | 60 (0.79) | 58 (0.77) | 58 (0.77) | 62 (0.82) | 60 (0.79) |
| | Second. rays | 94 (1.00) | 92 (0.98) | 103 (1.09) | 109 (1.16) | 118 (1.24) | 115 (1.22) | 131 (1.39) | 128 (1.35) | 120 (1.27) | 135 (1.43) |
| | Shadow rays | 221 (1.00) | 221 (1.00) | 254 (1.15) | 257 (1.16) | 267 (1.21) | 267 (1.21) | 290 (1.31) | 289 (1.31) | 275 (1.25) | 301 (1.37) |
| | Second. rays reord. | 96 (1.02) | 94 (1.00) | 105 (1.11) | 111 (1.18) | 119 (1.26) | 118 (1.25) | 134 (1.42) | 130 (1.38) | 123 (1.30) | 139 (1.47) |
| | Shadow rays reord. | 227 (1.03) | 226 (1.02) | 264 (1.20) | 269 (1.22) | 278 (1.26) | 276 (1.25) | 303 (1.37) | 300 (1.36) | 282 (1.28) | 310 (1.40) |
| Pompeii #triangles 5632k | BVH cost | 428 (1.00) | 314 (0.73) | 201 (0.47) | 173 (0.41) | 159 (0.37) | 159 (0.37) | 109 (0.26) | 109 (0.26) | 190 (0.44) | 120 (0.28) |
| | Second. rays | 86 (1.00) | 101 (1.17) | 123 (1.43) | 135 (1.57) | 145 (1.68) | 143 (1.66) | 229 (2.66) | 225 (2.61) | 145 (1.68) | 234 (2.71) |
| | Shadow rays | 190 (1.00) | 225 (1.19) | 290 (1.53) | 308 (1.62) | 326 (1.72) | 324 (1.71) | 472 (2.49) | 464 (2.44) | 317 (1.67) | 479 (2.52) |
| | Second. rays reord. | 89 (1.03) | 103 (1.19) | 126 (1.46) | 139 (1.61) | 149 (1.72) | 145 (1.69) | 227 (2.63) | 222 (2.58) | 147 (1.70) | 231 (2.68) |
| | Shadow rays reord. | 215 (1.13) | 251 (1.32) | 324 (1.70) | 344 (1.81) | 366 (1.93) | 356 (1.88) | 487 (2.56) | 480 (2.53) | 355 (1.87) | 500 (2.63) |
| San Miguel #triangles 7880k | BVH cost | 251 (1.00) | 183 (0.73) | 142 (0.56) | 136 (0.54) | 128 (0.51) | 125 (0.50) | 115 (0.46) | 115 (0.46) | 157 (0.63) | 133 (0.53) |
| | Second. rays | 72 (1.00) | 87 (1.21) | 103 (1.44) | 111 (1.55) | 128 (1.79) | 134 (1.87) | 150 (2.09) | 148 (2.06) | 120 (1.67) | 141 (1.97) |
| | Shadow rays | 194 (1.00) | 232 (1.20) | 309 (1.59) | 329 (1.70) | 340 (1.75) | 347 (1.79) | 378 (1.95) | 372 (1.92) | 330 (1.70) | 358 (1.85) |
| | Second. rays reord. | 84 (1.17) | 100 (1.39) | 121 (1.69) | 129 (1.80) | 148 (2.06) | 153 (2.13) | 171 (2.39) | 168 (2.35) | 141 (1.96) | 167 (2.33) |
| | Shadow rays reord. | 262 (1.35) | 313 (1.61) | 396 (2.04) | 426 (2.19) | 445 (2.30) | 448 (2.31) | 477 (2.46) | 469 (2.42) | 434 (2.24) | 467 (2.41) |
| Vienna #triangles 8637k | BVH cost | 299 (1.00) | 215 (0.72) | 135 (0.45) | 110 (0.37) | 101 (0.34) | 98 (0.33) | 80 (0.27) | 80 (0.27) | 115 (0.38) | 87 (0.29) |
| | Second. rays | 101 (1.00) | 103 (1.02) | 175 (1.74) | 192 (1.91) | 204 (2.03) | 212 (2.11) | 240 (2.38) | 237 (2.36) | 208 (2.07) | 236 (2.34) |
| | Shadow rays | 179 (1.00) | 194 (1.08) | 334 (1.86) | 357 (1.99) | 380 (2.12) | 382 (2.13) | 434 (2.42) | 430 (2.40) | 384 (2.14) | 437 (2.43) |
| | Second. rays reord. | 103 (1.02) | 106 (1.05) | 180 (1.79) | 194 (1.93) | 208 (2.07) | 213 (2.12) | 236 (2.35) | 234 (2.33) | 209 (2.08) | 233 (2.32) |
| | Shadow rays reord. | 195 (1.08) | 208 (1.16) | 367 (2.05) | 377 (2.10) | 402 (2.24) | 402 (2.24) | 438 (2.44) | 435 (2.42) | 400 (2.23) | 439 (2.45) |
| Powerplant #triangles 12759k | BVH cost | 124 (1.00) | 111 (0.90) | 78 (0.63) | 75 (0.61) | 69 (0.55) | 69 (0.42) | 52 (0.42) | 85 (0.69) | 58 (0.46) | |
| | Second. rays | 53 (1.00) | 60 (1.14) | 68 (1.28) | 81 (1.53) | 67 (1.27) | 65 (1.22) | 162 (3.05) | 165 (3.11) | 67 (1.26) | 191 (3.60) |
| | Shadow rays | 190 (1.00) | 207 (1.09) | 249 (1.31) | 250 (1.31) | 295 (1.55) | 264 (1.39) | 429 (2.26) | 421 (2.21) | 250 (1.31) | 433 (2.28) |
| | Second. rays reord. | 52 (0.98) | 61 (1.16) | 67 (1.26) | 80 (1.52) | 62 (1.17) | 60 (1.13) | 172 (3.25) | 173 (3.27) | 65 (1.23) | 201 (3.79) |
| | Shadow rays reord. | 224 (1.18) | 239 (1.25) | 269 (1.41) | 258 (1.36) | 344 (1.81) | 265 (1.39) | 444 (2.33) | 437 (2.30) | 273 (1.43) | 454 (2.39) |

Table 4. Performance comparison for all tested methods and scenes showing the BVH cost and trace speed in MRays/s for secondary and shadow rays with and without ray sorting using binary BVHs.

Wimmer for providing the Vienna and Pompeii scenes, and Morgan McGuire [2017] for providing the other scenes. This work was partly supported by the Czech Science Foundation (GA18-20374S) and Research Center for Informatics (CZ.02.1.01/0.0/0.0/16_019/0000765).

| Scene | Statistic | LBVH | HILBVH | PLOC | ATRBVH | PRBVH | PRBVH ^A | PRBVH _S | PRBVH _S ^A | SAH | SBVH |
|-------------------------------------|---------------------|------------|------------|------------|------------|-------------------|--------------------|--------------------|---------------------------------|------------|-------------------|
| Sibenik #triangles 75k | BVH cost | 108 (1.00) | 92 (0.85) | 90 (0.83) | 84 (0.78) | 80 (0.74) | 79 (0.74) | 76 (0.71) | 76 (0.70) | 84 (0.78) | 77 (0.71) |
| | Second. rays | 229 (1.00) | 266 (1.16) | 248 (1.08) | 280 (1.22) | 296 (1.29) | 300 (1.31) | 308 (1.35) | 307 (1.34) | 287 (1.25) | 307 (1.34) |
| | Shadow rays | 496 (1.00) | 541 (1.09) | 554 (1.12) | 583 (1.18) | 613 (1.24) | 630 (1.27) | 623 (1.26) | 620 (1.25) | 580 (1.17) | 597 (1.21) |
| | Second. rays reord. | 267 (1.16) | 304 (1.33) | 282 (1.23) | 317 (1.38) | 333 (1.45) | 337 (1.47) | 349 (1.52) | 348 (1.52) | 327 (1.42) | 349 (1.52) |
| | Shadow rays reord. | 626 (1.26) | 672 (1.36) | 688 (1.39) | 710 (1.43) | 742 (1.50) | 760 (1.53) | 743 (1.50) | 744 (1.50) | 712 (1.44) | 721 (1.46) |
| Crytek Sponza #triangles 262k | BVH cost | 163 (1.00) | 132 (0.81) | 118 (0.72) | 115 (0.71) | 115 (0.71) | 113 (0.70) | 107 (0.66) | 107 (0.66) | 131 (0.81) | 113 (0.70) |
| | Second. rays | 158 (1.00) | 180 (1.14) | 185 (1.17) | 197 (1.25) | 226 (1.43) | 226 (1.43) | 241 (1.53) | 238 (1.51) | 186 (1.18) | 230 (1.46) |
| | Shadow rays | 320 (1.00) | 376 (1.17) | 415 (1.30) | 445 (1.39) | 482 (1.50) | 480 (1.50) | 452 (1.41) | 455 (1.42) | 376 (1.18) | 420 (1.31) |
| | Second. rays reord. | 196 (1.24) | 226 (1.43) | 232 (1.47) | 242 (1.53) | 274 (1.74) | 276 (1.75) | 297 (1.88) | 293 (1.85) | 228 (1.45) | 284 (1.80) |
| | Shadow rays reord. | 419 (1.31) | 485 (1.52) | 519 (1.62) | 549 (1.71) | 591 (1.85) | 594 (1.86) | 562 (1.76) | 562 (1.76) | 482 (1.51) | 530 (1.65) |
| Conference #triangles 331k | BVH cost | 90 (1.00) | 74 (0.83) | 61 (0.68) | 61 (0.68) | 61 (0.68) | 60 (0.66) | 61 (0.68) | 61 (0.68) | 61 (0.68) | 63 (0.70) |
| | Second. rays | 256 (1.00) | 299 (1.17) | 359 (1.40) | 357 (1.39) | 368 (1.44) | 375 (1.46) | 384 (1.50) | 380 (1.48) | 356 (1.39) | 342 (1.34) |
| | Shadow rays | 484 (1.00) | 599 (1.24) | 698 (1.44) | 710 (1.47) | 758 (1.57) | 736 (1.52) | 738 (1.53) | 736 (1.52) | 658 (1.36) | 602 (1.24) |
| | Second. rays reord. | 317 (1.24) | 364 (1.42) | 423 (1.65) | 422 (1.65) | 434 (1.69) | 439 (1.71) | 455 (1.77) | 453 (1.77) | 425 (1.66) | 425 (1.66) |
| | Shadow rays reord. | 649 (1.34) | 778 (1.61) | 893 (1.85) | 906 (1.87) | 938 (1.94) | 907 (1.87) | 909 (1.88) | 905 (1.87) | 851 (1.76) | 790 (1.63) |
| Gallery #triangles 998k | BVH cost | 119 (1.00) | 117 (0.98) | 114 (0.96) | 104 (0.88) | 101 (0.85) | 99 (0.83) | 92 (0.78) | 92 (0.78) | 99 (0.84) | 93 (0.78) |
| | Second. rays | 134 (1.00) | 135 (1.01) | 139 (1.04) | 147 (1.10) | 153 (1.14) | 154 (1.15) | 161 (1.20) | 160 (1.20) | 153 (1.14) | 161 (1.20) |
| | Shadow rays | 290 (1.00) | 284 (0.98) | 305 (1.05) | 314 (1.08) | 330 (1.14) | 331 (1.14) | 338 (1.17) | 335 (1.15) | 320 (1.10) | 331 (1.14) |
| | Second. rays reord. | 146 (1.09) | 147 (1.10) | 153 (1.14) | 161 (1.20) | 167 (1.25) | 168 (1.26) | 173 (1.30) | 172 (1.29) | 168 (1.26) | 174 (1.30) |
| | Shadow rays reord. | 349 (1.20) | 340 (1.17) | 367 (1.26) | 374 (1.29) | 391 (1.35) | 393 (1.35) | 402 (1.38) | 399 (1.37) | 382 (1.32) | 392 (1.35) |
| Happy Buddha #triangles 1087k | BVH cost | 118 (1.00) | 110 (0.94) | 107 (0.91) | 103 (0.88) | 98 (0.83) | 96 (0.82) | 92 (0.79) | 92 (0.78) | 96 (0.82) | 93 (0.79) |
| | Second. rays | 118 (1.00) | 120 (1.01) | 119 (1.01) | 126 (1.06) | 131 (1.10) | 129 (1.09) | 135 (1.14) | 134 (1.13) | 132 (1.11) | 134 (1.13) |
| | Shadow rays | 169 (1.00) | 170 (1.01) | 177 (1.05) | 181 (1.07) | 186 (1.10) | 186 (1.10) | 190 (1.12) | 188 (1.12) | 187 (1.11) | 189 (1.12) |
| | Second. rays reord. | 114 (0.96) | 115 (0.97) | 115 (0.98) | 120 (1.01) | 124 (1.05) | 123 (1.04) | 127 (1.07) | 126 (1.07) | 125 (1.05) | 128 (1.08) |
| | Shadow rays reord. | 154 (0.91) | 155 (0.92) | 159 (0.94) | 163 (0.96) | 167 (0.99) | 166 (0.99) | 169 (1.00) | 169 (1.00) | 168 (1.00) | 170 (1.01) |
| Sodahall #triangles 2169k | BVH cost | 149 (1.00) | 134 (0.90) | 116 (0.77) | 110 (0.74) | 100 (0.67) | 100 (0.67) | 98 (0.66) | 98 (0.66) | 116 (0.78) | 104 (0.69) |
| | Second. rays | 212 (1.00) | 250 (1.18) | 245 (1.16) | 274 (1.29) | 314 (1.48) | 307 (1.45) | 334 (1.58) | 327 (1.54) | 283 (1.34) | 319 (1.50) |
| | Shadow rays | 484 (1.00) | 524 (1.08) | 557 (1.15) | 593 (1.23) | 604 (1.25) | 603 (1.25) | 599 (1.24) | 580 (1.20) | 575 (1.19) | 579 (1.20) |
| | Second. rays reord. | 234 (1.10) | 268 (1.26) | 264 (1.24) | 292 (1.38) | 326 (1.54) | 318 (1.50) | 342 (1.61) | 335 (1.58) | 299 (1.41) | 328 (1.55) |
| | Shadow rays reord. | 528 (1.09) | 556 (1.15) | 589 (1.22) | 620 (1.28) | 629 (1.30) | 624 (1.29) | 616 (1.27) | 601 (1.24) | 605 (1.25) | 602 (1.24) |
| Hairball #triangles 2880k | BVH cost | 922 (1.00) | 919 (1.00) | 797 (0.86) | 788 (0.85) | 742 (0.80) | 742 (0.80) | 608 (0.66) | 606 (0.66) | 802 (0.87) | 658 (0.71) |
| | Second. rays | 71 (1.00) | 72 (1.02) | 71 (1.00) | 83 (1.18) | 90 (1.28) | 90 (1.27) | 93 (1.32) | 92 (1.31) | 87 (1.23) | 90 (1.28) |
| | Shadow rays | 151 (1.00) | 154 (1.02) | 163 (1.07) | 177 (1.17) | 190 (1.25) | 188 (1.24) | 189 (1.25) | 186 (1.23) | 183 (1.21) | 184 (1.22) |
| | Second. rays reord. | 80 (1.13) | 82 (1.16) | 80 (1.14) | 94 (1.33) | 101 (1.43) | 100 (1.42) | 105 (1.49) | 103 (1.47) | 97 (1.37) | 102 (1.45) |
| | Shadow rays reord. | 173 (1.14) | 175 (1.16) | 191 (1.26) | 203 (1.34) | 216 (1.43) | 214 (1.42) | 210 (1.39) | 208 (1.38) | 210 (1.39) | 207 (1.37) |
| Crown #triangles 4868k | BVH cost | 46 (1.00) | 44 (0.96) | 42 (0.91) | 40 (0.87) | 39 (0.85) | 39 (0.84) | 38 (0.81) | 38 (0.81) | 40 (0.86) | 38 (0.83) |
| | Second. rays | 104 (1.00) | 104 (1.01) | 114 (1.11) | 118 (1.14) | 126 (1.21) | 125 (1.20) | 135 (1.30) | 131 (1.27) | 125 (1.21) | 135 (1.31) |
| | Shadow rays | 211 (1.00) | 215 (1.02) | 240 (1.14) | 242 (1.15) | 251 (1.19) | 252 (1.19) | 260 (1.23) | 256 (1.22) | 249 (1.18) | 261 (1.24) |
| | Second. rays reord. | 114 (1.10) | 115 (1.12) | 126 (1.22) | 130 (1.26) | 138 (1.33) | 136 (1.31) | 147 (1.42) | 145 (1.40) | 136 (1.32) | 148 (1.43) |
| | Shadow rays reord. | 220 (1.04) | 223 (1.06) | 249 (1.18) | 259 (1.23) | 258 (1.22) | 267 (1.27) | 265 (1.26) | 255 (1.21) | 268 (1.27) | |
| Pompeii #triangles 5632k | BVH cost | 255 (1.00) | 202 (0.79) | 151 (0.59) | 137 (0.54) | 130 (0.51) | 129 (0.51) | 81 (0.32) | 81 (0.32) | 136 (0.53) | 82 (0.32) |
| | Second. rays | 95 (1.00) | 111 (1.17) | 136 (1.44) | 153 (1.61) | 162 (1.70) | 160 (1.69) | 228 (2.40) | 224 (2.36) | 157 (1.65) | 230 (2.42) |
| | Shadow rays | 173 (1.00) | 213 (1.23) | 276 (1.60) | 292 (1.69) | 314 (1.82) | 310 (1.79) | 406 (2.35) | 400 (2.31) | 305 (1.76) | 414 (2.39) |
| | Second. rays reord. | 99 (1.05) | 116 (1.22) | 143 (1.50) | 156 (1.64) | 165 (1.74) | 164 (1.73) | 228 (2.40) | 223 (2.35) | 161 (1.70) | 230 (2.42) |
| | Shadow rays reord. | 192 (1.11) | 230 (1.33) | 292 (1.69) | 307 (1.78) | 326 (1.88) | 322 (1.86) | 409 (2.37) | 401 (2.32) | 320 (1.85) | 415 (2.40) |
| San Miguel #triangles 7880k | BVH cost | 146 (1.00) | 117 (0.80) | 98 (0.67) | 96 (0.66) | 92 (0.63) | 90 (0.62) | 82 (0.56) | 82 (0.56) | 102 (0.69) | 86 (0.59) |
| | Second. rays | 69 (1.00) | 86 (1.25) | 103 (1.49) | 107 (1.55) | 116 (1.68) | 121 (1.75) | 131 (1.90) | 131 (1.90) | 106 (1.53) | 128 (1.85) |
| | Shadow rays | 174 (1.00) | 217 (1.25) | 255 (1.46) | 264 (1.51) | 276 (1.59) | 276 (1.59) | 296 (1.70) | 293 (1.68) | 267 (1.53) | 288 (1.65) |
| | Second. rays reord. | 82 (1.19) | 102 (1.47) | 119 (1.73) | 124 (1.80) | 135 (1.95) | 140 (2.02) | 151 (2.18) | 150 (2.17) | 125 (1.80) | 147 (2.13) |
| | Shadow rays reord. | 224 (1.29) | 269 (1.54) | 310 (1.78) | 322 (1.85) | 333 (1.91) | 332 (1.91) | 350 (2.01) | 347 (1.99) | 324 (1.86) | 345 (1.98) |
| Vienna #triangles 8637k | BVH cost | 163 (1.00) | 124 (0.76) | 89 (0.54) | 77 (0.47) | 71 (0.44) | 70 (0.43) | 52 (0.32) | 52 (0.32) | 77 (0.47) | 54 (0.33) |
| | Second. rays | 106 (1.00) | 118 (1.11) | 170 (1.60) | 184 (1.74) | 201 (1.89) | 204 (1.92) | 227 (2.14) | 225 (2.11) | 194 (1.83) | 219 (2.06) |
| | Shadow rays | 166 (1.00) | 195 (1.18) | 291 (1.75) | 318 (1.92) | 339 (2.05) | 346 (2.08) | 375 (2.26) | 370 (2.23) | 331 (2.00) | 367 (2.21) |
| | Second. rays reord. | 114 (1.07) | 127 (1.19) | 178 (1.67) | 193 (1.81) | 208 (1.96) | 210 (1.97) | 232 (2.19) | 231 (2.17) | 199 (1.88) | 224 (2.11) |
| | Shadow rays reord. | 182 (1.10) | 210 (1.26) | 303 (1.83) | 327 (1.97) | 347 (2.09) | 351 (2.11) | 376 (2.27) | 373 (2.25) | 338 (2.03) | 368 (2.22) |
| Powerplant #triangles 12759k | BVH cost | 75 (1.00) | 70 (0.93) | 55 (0.73) | 54 (0.72) | 51 (0.68) | 50 (0.67) | 36 (0.49) | 36 (0.48) | 57 (0.76) | 37 (0.49) |
| | Second. rays | 81 (1.00) | 92 (1.14) | 116 (1.44) | 115 (1.43) | 119 (1.48) | 120 (1.49) | 196 (2.43) | 195 (2.42) | 108 (1.34) | 203 (2.52) |
| | Shadow rays | 231 (1.00) | 248 (1.07) | 310 (1.34) | 312 (1.35) | 340 (1.47) | 340 (1.47) | 392 (1.69) | 382 (1.65) | 295 (1.28) | 388 (1.68) |
| | Second. rays reord. | 94 (1.17) | 106 (1.31) | 128 (1.59) | 128 (1.59) | 128 (1.59) | 129 (1.60) | 211 (2.62) | 207 (2.57) | 120 (1.49) | 215 (2.67) |
| | Shadow rays reord. | 259 (1.12) | 275 (1.19) | 335 (1.45) | 333 (1.44) | 361 (1.56) | 361 (1.56) | 397 (1.71) | 387 (1.67) | 326 (1.41) | 395 (1.71) |

Copyright Notice and Trademarks

©2022 Advanced Micro Devices, Inc. All rights reserved. AMD, Ryzen, Radeon, and combinations thereof are trademarks of Advanced Micro Devices, Inc. Other product names used in this publication are for identification purposes only and may

| Scene | Statistic | LBVH | HLBVH | PLOC | ATRBVH | PRBVH | PRBVH ^A | PRBVH _S | PRBVH _S ^A | SAH | SBVH |
|-------------------------------------|---------------------|------------|------------|------------|------------|-------------------|--------------------|--------------------|---------------------------------|------------------|-------------------|
| Sibenik #triangles 75k | BVH cost | 113 (1.00) | 102 (0.90) | 97 (0.86) | 94 (0.83) | 91 (0.81) | 90 (0.80) | 85 (0.76) | 85 (0.76) | 92 (0.82) | 84 (0.74) |
| | Second. rays | 197 (1.00) | 222 (1.13) | 215 (1.09) | 234 (1.19) | 244 (1.24) | 247 (1.26) | 253 (1.29) | 253 (1.28) | 233 (1.19) | 250 (1.27) |
| | Shadow rays | 439 (1.00) | 449 (1.02) | 475 (1.08) | 472 (1.07) | 500 (1.14) | 508 (1.16) | 515 (1.17) | 516 (1.18) | 486 (1.11) | 482 (1.10) |
| | Second. rays reord. | 225 (1.14) | 250 (1.27) | 240 (1.22) | 261 (1.33) | 273 (1.39) | 275 (1.40) | 282 (1.44) | 282 (1.43) | 262 (1.33) | 280 (1.42) |
| | Shadow rays reord. | 497 (1.13) | 505 (1.15) | 531 (1.21) | 524 (1.19) | 555 (1.26) | 562 (1.28) | 565 (1.29) | 568 (1.29) | 540 (1.23) | 533 (1.21) |
| Crytek Sponza #triangles 262k | BVH cost | 176 (1.00) | 142 (0.81) | 137 (0.78) | 136 (0.77) | 135 (0.77) | 133 (0.76) | 129 (0.73) | 128 (0.73) | 136 (0.77) | 130 (0.74) |
| | Second. rays | 130 (1.00) | 151 (1.16) | 159 (1.22) | 172 (1.32) | 194 (1.49) | 198 (1.52) | 200 (1.54) | 199 (1.53) | 156 (1.20) | 190 (1.46) |
| | Shadow rays | 279 (1.00) | 326 (1.17) | 345 (1.24) | 376 (1.35) | 425 (1.52) | 431 (1.54) | 374 (1.34) | 375 (1.35) | 313 (1.12) | 348 (1.25) |
| | Second. rays reord. | 158 (1.21) | 183 (1.41) | 189 (1.45) | 203 (1.56) | 228 (1.75) | 232 (1.78) | 237 (1.82) | 235 (1.81) | 188 (1.44) | 227 (1.74) |
| | Shadow rays reord. | 326 (1.17) | 373 (1.34) | 393 (1.41) | 428 (1.54) | 477 (1.71) | 484 (1.73) | 422 (1.51) | 420 (1.51) | 360 (1.29) | 396 (1.42) |
| Conference #triangles 331k | BVH cost | 91 (1.00) | 83 (0.91) | 75 (0.83) | 75 (0.82) | 75 (0.83) | 75 (0.83) | 78 (0.86) | 78 (0.86) | 70 (0.77) | 75 (0.82) |
| | Second. rays | 242 (1.00) | 274 (1.13) | 322 (1.33) | 328 (1.36) | 334 (1.38) | 335 (1.38) | 322 (1.33) | 320 (1.32) | 318 (1.31) | 292 (1.21) |
| | Shadow rays | 481 (1.00) | 557 (1.16) | 638 (1.33) | 643 (1.44) | 655 (1.36) | 659 (1.37) | 622 (1.29) | 621 (1.29) | 583 (1.21) | 539 (1.12) |
| | Second. rays reord. | 287 (1.19) | 322 (1.33) | 367 (1.52) | 371 (1.54) | 381 (1.58) | 379 (1.57) | 369 (1.52) | 366 (1.51) | 367 (1.52) | 350 (1.45) |
| | Shadow rays reord. | 544 (1.13) | 634 (1.32) | 720 (1.50) | 717 (1.49) | 738 (1.53) | 738 (1.53) | 685 (1.42) | 682 (1.42) | 658 (1.37) | 615 (1.28) |
| Gallery #triangles 998k | BVH cost | 119 (1.00) | 117 (0.99) | 111 (0.94) | 106 (0.89) | 101 (0.85) | 99 (0.83) | 93 (0.78) | 92 (0.78) | 100 (0.84) | 93 (0.78) |
| | Second. rays | 114 (1.00) | 116 (1.02) | 117 (1.03) | 126 (1.11) | 130 (1.14) | 131 (1.15) | 140 (1.23) | 139 (1.22) | 131 (1.15) | 139 (1.22) |
| | Shadow rays | 252 (1.00) | 249 (0.99) | 267 (1.06) | 282 (1.12) | 287 (1.14) | 295 (1.17) | 305 (1.21) | 305 (1.21) | 286 (1.14) | 302 (1.20) |
| | Second. rays reord. | 126 (1.10) | 128 (1.12) | 131 (1.15) | 140 (1.23) | 143 (1.26) | 147 (1.29) | 154 (1.35) | 153 (1.34) | 147 (1.29) | 153 (1.34) |
| | Shadow rays reord. | 283 (1.12) | 278 (1.10) | 301 (1.19) | 315 (1.25) | 321 (1.28) | 330 (1.31) | 341 (1.35) | 341 (1.35) | 320 (1.27) | 337 (1.34) |
| Happy Buddha #triangles 1087k | BVH cost | 115 (1.00) | 111 (0.97) | 105 (0.91) | 102 (0.89) | 97 (0.85) | 95 (0.83) | 92 (0.80) | 92 (0.80) | 96 (0.84) | 93 (0.81) |
| | Second. rays | 115 (1.00) | 116 (1.01) | 116 (1.02) | 122 (1.06) | 128 (1.12) | 127 (1.11) | 131 (1.14) | 131 (1.14) | 129 (1.12) | 131 (1.14) |
| | Shadow rays | 158 (1.00) | 159 (1.00) | 163 (1.03) | 170 (1.07) | 174 (1.10) | 174 (1.10) | 176 (1.12) | 175 (1.11) | 174 (1.11) | 175 (1.11) |
| | Second. rays reord. | 109 (0.95) | 110 (0.96) | 110 (0.96) | 115 (1.01) | 119 (1.03) | 119 (1.04) | 122 (1.06) | 121 (1.06) | 119 (1.04) | 122 (1.06) |
| | Shadow rays reord. | 141 (0.90) | 143 (0.90) | 146 (0.92) | 151 (0.96) | 154 (0.98) | 154 (0.98) | 156 (0.99) | 155 (0.98) | 154 (0.97) | 156 (0.99) |
| Sodahall #triangles 2169k | BVH cost | 153 (1.00) | 142 (0.93) | 126 (0.82) | 122 (0.79) | 115 (0.75) | 115 (0.75) | 112 (0.73) | 112 (0.73) | 119 (0.78) | 111 (0.73) |
| | Second. rays | 185 (1.00) | 224 (1.21) | 214 (1.16) | 239 (1.29) | 274 (1.48) | 272 (1.47) | 278 (1.50) | 276 (1.49) | 244 (1.32) | 269 (1.45) |
| | Shadow rays | 394 (1.00) | 436 (1.11) | 462 (1.17) | 468 (1.19) | 496 (1.26) | 498 (1.27) | 480 (1.22) | 478 (1.21) | 467 (1.19) | 469 (1.19) |
| | Second. rays reord. | 201 (1.09) | 238 (1.29) | 229 (1.24) | 250 (1.35) | 282 (1.53) | 282 (1.52) | 286 (1.55) | 283 (1.53) | 256 (1.39) | 277 (1.50) |
| | Shadow rays reord. | 408 (1.04) | 443 (1.12) | 468 (1.19) | 470 (1.19) | 493 (1.25) | 495 (1.26) | 480 (1.22) | 476 (1.21) | 470 (1.19) | 470 (1.19) |
| Hairball #triangles 2880k | BVH cost | 979 (1.00) | 979 (1.00) | 828 (0.85) | 828 (0.85) | 781 (0.80) | 780 (0.80) | 621 (0.63) | 624 (0.64) | 825 (0.84) | 632 (0.65) |
| | Second. rays | 70 (1.00) | 72 (1.02) | 66 (0.94) | 79 (1.12) | 84 (1.19) | 83 (1.18) | 91 (1.29) | 89 (1.27) | 80 (1.14) | 86 (1.22) |
| | Shadow rays | 157 (1.00) | 160 (1.02) | 161 (1.03) | 175 (1.11) | 181 (1.15) | 180 (1.14) | 188 (1.20) | 186 (1.18) | 176 (1.12) | 180 (1.15) |
| | Second. rays reord. | 79 (1.12) | 80 (1.13) | 75 (1.06) | 88 (1.25) | 93 (1.32) | 92 (1.31) | 101 (1.43) | 99 (1.40) | 89 (1.27) | 96 (1.36) |
| | Shadow rays reord. | 170 (1.08) | 173 (1.10) | 177 (1.12) | 189 (1.20) | 195 (1.24) | 193 (1.23) | 200 (1.27) | 198 (1.26) | 189 (1.20) | 192 (1.22) |
| Crown #triangles 4868k | BVH cost | 47 (1.00) | 46 (0.98) | 43 (0.91) | 42 (0.90) | 41 (0.87) | 41 (0.87) | 39 (0.84) | 39 (0.84) | 41 (0.88) | 40 (0.84) |
| | Second. rays | 100 (1.00) | 100 (1.00) | 108 (1.08) | 112 (1.12) | 118 (1.18) | 117 (1.17) | 125 (1.25) | 124 (1.24) | 116 (1.16) | 124 (1.24) |
| | Shadow rays | 201 (1.00) | 202 (1.01) | 220 (1.10) | 224 (1.12) | 230 (1.14) | 232 (1.15) | 235 (1.17) | 236 (1.17) | 227 (1.13) | 233 (1.16) |
| | Second. rays reord. | 108 (1.08) | 108 (1.08) | 116 (1.16) | 121 (1.21) | 126 (1.26) | 125 (1.25) | 133 (1.33) | 132 (1.32) | 125 (1.25) | 133 (1.32) |
| | Shadow rays reord. | 198 (0.99) | 199 (0.99) | 216 (1.07) | 220 (1.09) | 225 (1.12) | 226 (1.12) | 231 (1.15) | 231 (1.15) | 223 (1.11) | 229 (1.14) |
| Pompeii #triangles 5632k | BVH cost | 250 (1.00) | 222 (0.89) | 169 (0.68) | 157 (0.63) | 151 (0.60) | 151 (0.60) | 92 (0.37) | 92 (0.37) | 147 (0.59) | 87 (0.35) |
| | Second. rays | 87 (1.00) | 103 (1.18) | 129 (1.48) | 141 (1.62) | 152 (1.75) | 151 (1.73) | 204 (2.34) | 201 (2.31) | 146 (1.67) | 205 (2.35) |
| | Shadow rays | 160 (1.00) | 192 (1.20) | 242 (1.51) | 261 (1.63) | 272 (1.70) | 271 (1.69) | 344 (2.15) | 339 (2.12) | 265 (1.65) | 345 (2.16) |
| | Second. rays reord. | 90 (1.03) | 105 (1.21) | 132 (1.51) | 143 (1.64) | 152 (1.75) | 151 (1.74) | 202 (2.32) | 199 (2.28) | 147 (1.69) | 204 (2.34) |
| | Shadow rays reord. | 164 (1.03) | 194 (1.21) | 242 (1.51) | 259 (1.62) | 268 (1.67) | 267 (1.67) | 333 (2.08) | 327 (2.04) | 262 (1.64) | 335 (2.09) |
| San Miguel #triangles 7880k | BVH cost | 149 (1.00) | 128 (0.86) | 110 (0.74) | 109 (0.73) | 105 (0.70) | 104 (0.70) | 93 (0.63) | 93 (0.63) | 110 (0.74) | 93 (0.62) |
| | Second. rays | 67 (1.00) | 79 (1.18) | 93 (1.39) | 97 (1.45) | 106 (1.58) | 111 (1.65) | 120 (1.79) | 117 (1.75) | 95 (1.42) | 110 (1.64) |
| | Shadow rays | 170 (1.00) | 202 (1.19) | 238 (1.40) | 242 (1.42) | 253 (1.49) | 255 (1.50) | 271 (1.59) | 266 (1.57) | 244 (1.44) | 252 (1.48) |
| | Second. rays reord. | 77 (1.16) | 91 (1.36) | 106 (1.58) | 111 (1.66) | 121 (1.80) | 126 (1.88) | 134 (2.01) | 131 (1.96) | 110 (1.64) | 127 (1.89) |
| | Shadow rays reord. | 197 (1.16) | 231 (1.36) | 270 (1.59) | 276 (1.63) | 285 (1.68) | 287 (1.69) | 301 (1.77) | 297 (1.75) | 280 (1.65) | 287 (1.69) |
| Vienna #triangles 8637k | BVH cost | 145 (1.00) | 123 (0.85) | 87 (0.60) | 76 (0.53) | 71 (0.49) | 70 (0.49) | 54 (0.37) | 54 (0.37) | 74 (0.51) | 54 (0.37) |
| | Second. rays | 102 (1.00) | 113 (1.11) | 156 (1.53) | 174 (1.70) | 189 (1.85) | 193 (1.89) | 209 (2.04) | 207 (2.02) | 180 (1.76) | 202 (1.97) |
| | Shadow rays | 164 (1.00) | 192 (1.18) | 260 (1.59) | 287 (1.75) | 307 (1.88) | 310 (1.89) | 328 (2.00) | 325 (1.99) | 295 (1.80) | 323 (1.97) |
| | Second. rays reord. | 108 (1.05) | 119 (1.16) | 160 (1.57) | 178 (1.74) | 192 (1.87) | 194 (1.89) | 210 (2.05) | 207 (2.02) | 182 (1.78) | 203 (1.98) |
| | Shadow rays reord. | 167 (1.02) | 193 (1.18) | 256 (1.57) | 281 (1.72) | 299 (1.83) | 300 (1.83) | 318 (1.94) | 314 (1.92) | 287 (1.75) | 313 (1.91) |
| Powerplant #triangles 12759k | BVH cost | 70 (1.00) | 67 (0.96) | 55 (0.79) | 55 (0.79) | 53 (0.76) | 53 (0.75) | 38 (0.55) | 38 (0.55) | 55 (0.78) | 37 (0.52) |
| | Second. rays | 84 (1.00) | 96 (1.14) | 120 (1.42) | 129 (1.54) | 133 (1.58) | 141 (1.67) | 183 (2.18) | 180 (2.13) | 119 (1.41) | 184 (2.19) |
| | Shadow rays | 223 (1.00) | 241 (1.08) | 286 (1.29) | 293 (1.32) | 307 (1.38) | 316 (1.42) | 341 (1.53) | 336 (1.51) | 277 (1.25) | 339 (1.52) |
| | Second. rays reord. | 97 (1.15) | 108 (1.28) | 131 (1.55) | 141 (1.68) | 149 (1.77) | 156 (1.86) | 191 (2.27) | 187 (2.22) | 132 (1.57) | 192 (2.28) |
| | Shadow rays reord. | 233 (1.05) | 249 (1.12) | 293 (1.32) | 297 (1.33) | 313 (1.41) | 317 (1.42) | 337 (1.52) | 332 (1.49) | 284 (1.27) | 335 (1.50) |

Table 6. Performance comparison for all tested methods and scenes showing the BVH cost and trace speed in MRays/s for secondary and shadow rays with and without ray sorting using octal BVHs.

be trademarks of their respective companies.

References

- AILA, T., AND LAINE, S. 2009. Understanding the Efficiency of Ray Traversal on GPUs. In

- Proceedings of High-Performance Graphics*, 145–149. URL: <https://doi.org/10.1145/1572769.1572792>. 6, 7, 9, 10
- AILA, T., KARRAS, T., AND LAINE, S. 2013. On Quality Metrics of Bounding Volume Hierarchies. In *Proceedings of High-Performance Graphics*, 101–108. URL: <https://doi.org/10.1145/2492045.2492056>. 2, 10
- DOMINGUES, L., AND PEDRINI, H. 2015. Bounding Volume Hierarchy Optimization through Agglomerative Treelet Restructuring. In *Proceedings of High-Performance Graphics*, 13–20. URL: <https://doi.org/10.1145/2790060.2790065>. 5, 7
- GARANZHA, K., PANTALEONI, J., AND MCALLISTER, D. 2011. Simpler and Faster HLBVH with Work Queues. In *Proceedings of High-Performance Graphics*, 59–64. URL: <https://doi.org/10.1145/964965.808590>. 4, 7
- GOLDSMITH, J., AND SALMON, J. 1987. Automatic Creation of Object Hierarchies for Ray Tracing. *Computer Graphics and Applications* 7, 5, 14–20. URL: <https://ieeexplore.ieee.org/document/4057175>. 3
- KARRAS, T., AND AILA, T. 2013. Fast Parallel Construction of High-Quality Bounding Volume Hierarchies. In *Proceedings of High-Performance Graphics*, 89–100. URL: <https://doi.org/10.1145/2492045.2492055>. 4
- KARRAS, T. 2012. Maximizing Parallelism in the Construction of BVHs, Octrees, and k-d Trees. In *Proceedings of High-Performance Graphics*, 33–37. URL: <https://research.nvidia.com/publication/maximizing-parallelism-construction-bvhs-octrees-and-k-d-trees>. 4, 7
- KENSLER, A. 2008. Tree Rotations for Improving Bounding Volume Hierarchies. In *Proceedings of Symposium on Interactive Ray Tracing*, 73–76. URL: <https://ieeexplore.ieee.org/document/4634624>. 5
- LIER, A., STAMMINGER, M., AND SELGRAD, K. 2018. CPU-style SIMD Ray Traversal on GPUs. In *Proceedings of High-Performance Graphics*, 7:1–7:4. URL: <https://doi.org/10.1145/3231578.3231583>. 7, 9, 10
- MCGUIRE, M., 2017. Computer Graphics Archive, July. URL: <https://casual-effects.com/data>. 14
- MEISTER, D., AND BITTNER, J. 2018. Parallel Locally-Ordered Clustering for Bounding Volume Hierarchy Construction. *IEEE Transactions on Visualization and Computer Graphics* 24, 3, 1345–1353. URL: <https://doi.org/10.1109/TVCG.2017.2669983>. 4, 7
- MEISTER, D., AND BITTNER, J. 2018. Parallel Reinsertion for Bounding Volume Hierarchy Optimization. *Computer Graphics Forum (Proceedings of Eurographics)* 37, 2, 463–473. URL: <https://diglib.eg.org:443/handle/10.1111/cgf13376>. 5, 6, 7
- MEISTER, D., BOKŠANSKÝ, J., GUTHE, M., AND BITTNER, J. 2020. On Ray Reordering Techniques for Faster GPU Ray Tracing. In *Proceedings of Symposium on Interactive 3D Graphics and Games*. URL: <https://doi.org/10.1145/3384382.3384534>. 7, 8

- MEISTER, D., OGAKI, S., BENTHIN, C., DOYLE, M. J., GUTHE, M., AND BITTNER, J. 2021. A Survey on Bounding Volume Hierarchies for Ray Tracing. *Computer Graphics Forum (Proceedings of Eurographics)* 40, 2. URL: <https://onlinelibrary.wiley.com/doi/abs/10.1111/cgf.142662>. 2, 13
- MERRILL, D., AND GRIMSHAW, A. 2011. High Performance and Scalable Radix Sorting: A case study of implementing dynamic parallelism for GPU computing. *Parallel Processing Letters* 21, 2, 245–272. URL: <https://doi.org/10.1142/S0129626411000187>. 8
- MORTON, G. 1966. A Computer Oriented Geodetic Database and a New Technique in File Sequencing. Tech. rep. URL: <https://dominoweb.draco.res.ibm.com/0dabf9473b9c86d48525779800566a39.html>. 4
- PANTALEONI, J., AND LUEBKE, D. 2010. HLBVH: Hierarchical LBVH Construction for Real-Time Ray Tracing of Dynamic Geometry. In *Proceedings of High-Performance Graphics*, 87–95. URL: <https://research.nvidia.com/publication/hlbvh-hierarchical-lbvh-construction-real-time-ray-tracing>. 4
- STICH, M., FRIEDRICH, H., AND DIETRICH, A. 2009. Spatial Splits in Bounding Volume Hierarchies. In *Proceedings of the High-Performance Graphics*, 7–13. URL: <https://doi.org/10.1145/1572769.1572771>. 6, 7
- VINKLER, M., HAVRAN, V., AND BITTNER, J. 2016. Performance Comparison of Bounding Volume Hierarchies and Kd-Trees for GPU Ray Tracing. *Computer Graphics Forum*. URL: <https://onlinelibrary.wiley.com/doi/abs/10.1111/cgf.12776>. 2
- WALD, I., BENTHIN, C., AND BOULOS, S. 2008. Getting Rid of Packets - Efficient SIMD Single-Ray Traversal using Multi-Branching BVHs. In *Symposium on Interactive Ray Tracing*, 49–57. URL: <https://doi.org/10.1145/3105762.3105773>. 3
- YLITIE, H., KARRAS, T., AND LAINE, S. 2017. Efficient Incoherent Ray Traversal on GPUs Through Compressed Wide BVHs. In *Proceedings of High-Performance Graphics*, 4:1–4:13. URL: <https://doi.org/10.1145/3105762.3105773>. 7, 9

Index of Supplemental Materials

The source codes of the algorithm can be downloaded from Github: <https://github.com/meistdan/hippie>

Author Contact Information

Daniel Meister
AMD Japan Co. Ltd.
Marunouchi Trust Tower
1-8-3 Marunouchi, Chiyoda-ku
Tokyo, Japan
daniel.meister@amd.com
<https://meistdan.github.io>

Jiří Bittner
Czech Technical University in Prague
Karlovo náměstí 13
121 35 Prague 2
Prague, Czech Republic
bittner@fel.cvut.cz
<https://dcgi.fel.cvut.cz/home/bittner>

Daniel Meister, Jiří Bittner, Performance Comparison of Bounding Volume Hierarchies for GPU Ray Tracing, *Journal of Computer Graphics Techniques (JCGT)*, vol. ?, no. ?, 1–1, ????
????

Received: July 8, 2022

Recommended: ????-??-?? Corresponding Editor: ??? ???

Published: ????-??-?? Editor-in-Chief: Marc Olano

© ???? Daniel Meister, Jiří Bittner (the Authors).

The Authors provide this document (the Work) under the Creative Commons CC BY-ND 3.0 license available online at <http://creativecommons.org/licenses/by-nd/3.0/>. The Authors further grant permission for reuse of images and text from the first page of the Work, provided that the reuse is for the purpose of promoting and/or summarizing the Work in scholarly venues and that any reuse is accompanied by a scientific citation to the Work.

